

MADPH 01-1226
BNL-HET-01/15
MSUHEP-10510
DFTT 13/2001
hep-ph/0105129

$H + 2$ JETS VIA GLUON FUSION

V. Del Duca^a, W. Kilgore^b, C. Oleari^c, C. Schmidt^d and D. Zeppenfeld^c

^(a) *I.N.F.N., Sezione di Torino via P. Giuria, 1 - 10125 Torino, Italy*

^(b) *Physics Department, Brookhaven National Laboratory, Upton, New York 11973, U.S.A.*

^(c) *Department of Physics, University of Wisconsin, Madison, WI 53706, U.S.A.*

^(d) *Department of Physics and Astronomy, Michigan State University, East Lansing, MI 48824, U.S.A.*

Abstract

Real emission corrections to $gg \rightarrow H$, which lead to $H + 2$ jet events, are calculated at order α_s^4 . Contributions include top-quark triangles, boxes and pentagon diagrams and are evaluated analytically for arbitrary top mass m_t . This new source of $H + 2$ jet events is compared to the weak-boson fusion cross section for a range of Higgs boson masses. The heavy top-mass approximation appears to work well for intermediate Higgs-boson masses, provided that the transverse momenta of the final-state partons are smaller than the top-quark mass.

1 Introduction

Gluon fusion via a top-quark loop is expected to be the most copious source of Higgs bosons in high energy hadronic collisions. Because of its importance for Higgs searches at the CERN LHC [1, 2], precise knowledge of higher order QCD corrections will be crucial to predict event characteristics for a Higgs signal, and to extract Higgs properties, like Higgs couplings to gauge bosons and fermions [3].

For the measurement of Higgs boson couplings, the separation of different Higgs production processes is necessary. Weak-boson fusion (WBF), i.e. the radiation of a Higgs boson from a t -channel W or Z boson in electroweak quark-quark scattering, is characterized by the presence of two forward jets. Such $H + 2$ jet events can also arise from $\mathcal{O}(\alpha_s^2)$ corrections to gluon fusion. For a measurement of WBF cross sections, the “background” from this latter process must be known, i.e. we need to calculate the cross section and event characteristics of $H + 2$ jet events arising from gluon fusion.

Next-to-leading order (NLO) QCD corrections to the inclusive gluon-fusion cross section are known to be large, leading to a K -factor close to two [4]. Because the lowest order process is loop induced, a full NNLO calculation would entail a three-loop evaluation, which presently is not feasible. Fortunately, for the intermediate Higgs mass range, which is the focus of present interest, the Higgs boson mass m_H is small compared to the top-quark pair threshold and the large m_t limit promises to be an adequate approximation. Consequently, present efforts on a NNLO calculation of the inclusive gluon-fusion cross section concentrate on the $m_t \rightarrow \infty$ limit, in which the task reduces to an effective two-loop calculation [5]. In order to assess the validity of this approximation, gluon-fusion cross-section calculations, which include all finite m_t corrections, are needed. Of particular interest are phase space regions where one or several of the kinematical invariants are of the order of, or exceed, the top-quark mass, i.e. regions of large Higgs boson or jet transverse momenta, or regions where dijet invariant masses become large.

In this letter we present first results of such a calculation, namely the evaluation of the real emission corrections to gluon fusion which lead to $H + 2$ parton final states, at order α_s^4 . This includes the subprocesses

$$qQ \rightarrow qQH, \quad qg \rightarrow qgH, \quad gg \rightarrow ggH, \quad (1.1)$$

and all crossing-related processes. The corresponding scattering amplitudes, involving triangle, box and pentagon diagrams with a top-quark loop, are calculated analytically for arbitrary values of the top-quark mass.

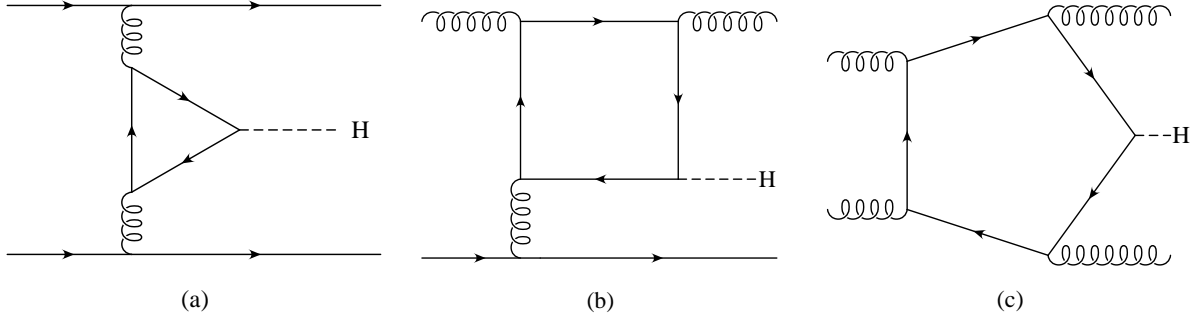


Figure 1: *Samples of Feynman graphs contributing to $H + 2$ jet production via gluon fusion.*

2 Calculation

In Fig. 1 we have collected a few representative Feynman diagrams that occur in Higgs production plus two jets, at order α_s^4 . In our calculation, the top quark is treated as massive but we neglect all other quark masses, so that the Higgs couples to gluons only via a top-quark loop. Typically we have a ggH coupling through a triangle loop (Fig. 1 (a)), a $gggH$ coupling through a box loop (Fig. 1 (b)) and a $ggggH$ one through a pentagon loop (Fig. 1 (c)).

The number and type of diagrams can be easily traced back if one thinks to insert these Higgs-gluon “vertices” into the tree-level diagrams for $2 \rightarrow 2$ QCD parton scattering. In the following counting, we exploit Furry’s theorem, i.e. we are counting as one the two charge-conjugation related diagrams where the loop momentum is running clockwise and counter-clockwise. This halves the number of diagrams. In addition, the crossed processes are not listed as extra diagrams, but are included in the final results.

1. $qQ \rightarrow qQH$ There is only one diagram obtained from the insertion of a triangle loop into the tree-level diagram $qQ \rightarrow qQ$, i.e. Fig. 1 (a).
2. $qg \rightarrow qgH$ At tree level, there are 3 diagrams contributing to the process $qg \rightarrow qg$: one with a three-gluon vertex and two Compton-like ones. Inserting a triangle loop into every gluon line, we have a total of 7 different diagrams. In addition, we can insert a box loop into the diagram with the three-gluon vertex, in 3 different ways: the 3! permutations of the 3 gluons are reduced to 3 graphs by using Furry’s theorem. In total we have 10 different diagrams for the $qg \rightarrow qgH$ contribution.
3. $gg \rightarrow ggH$ Four diagrams contribute to the tree-level scattering process $gg \rightarrow gg$: a four-gluon vertex diagram and 3 diagrams with two three-gluon vertices each. Inserting a triangle loop in any of the gluonic legs, gives rise to 19 different diagrams. The

insertion of the box loop in the 3 diagrams with three-gluon vertices yields another 18 diagrams. Finally, there are 12 pentagon diagrams (corresponding to $4!$ permutations of the external gluons, divided by 2, according to Furry's theorem).

The procedure for computing these diagrams is outlined below. A detailed discussion is postponed to a later paper [6].

Tensor integrals Triangle and box integrals are evaluated in terms of Passarino-Veltman C_{ij} and D_{ij} functions [7]. Gluon polarization vectors are expressed in terms of external momenta, which substantially simplifies expressions. Helicity techniques are employed for the numerical evaluation of all amplitudes involving external quarks.

In case of the pentagon diagrams appearing in the $ggggH$ amplitudes, the four external gluon-momenta form a basis in terms of which we expand the gluon polarization vectors. In this way, all the scalar products appearing in the numerator of the tensor integrals are products of the external momenta and the loop momentum (k). These dot products are then written as a difference of two propagators, plus a k -independent term. In this way, tensor pentagon integrals are transformed into a linear combination of tensor boxes and of scalar pentagons.

Scalar integrals All the scalar integrals needed for the calculation are finite in $D = 4$ dimensions, due to the presence of the top-quark mass. No further regulator is required. Scalar triangles and boxes have been known for a long time in the literature [8] and efficient computational procedures are available [9]. Following the procedure outlined in Refs. [10], we have expressed all scalar pentagons as linear combinations of scalar boxes.

Checks We were able to perform two different kinds of checks on the analytic amplitudes we computed:

1. *Gauge invariance*: an important test of the calculation is the gauge invariance of the amplitudes for $qg \rightarrow qgH$ and $gg \rightarrow ggH$. This test was performed both analytically and numerically, in the final Fortran program.
2. *Large m_t limit*: the amplitudes for Higgs plus two partons agree in the large m_t limit with the corresponding amplitudes obtained from the heavy-top effective Lagrangian [11]. This was done numerically by setting $m_t = 3$ TeV. We found agreement within a few percent, when the Higgs mass is varied in the range $100 \text{ GeV} < m_H < 700 \text{ GeV}$.

3 Discussion of the results

The gluon-fusion processes at $\mathcal{O}(\alpha_s^4)$, together with weak-boson fusion ($qQ \rightarrow qQH$ production via t -channel exchange of a W or Z), are expected to be the dominant sources of $H + 2$ jet events at the LHC. Cross sections for the former diverge as the final-state partons become collinear with one another or with the incident beam directions, or as final-state gluons become soft. A minimal set of cuts on the final-state partons, which anticipates LHC detector capabilities and jet finding algorithms, is required to define an $H + 2$ jet cross section. Our minimal set of cuts is

$$p_{Tj} > 20 \text{ GeV}, \quad |\eta_j| < 5, \quad R_{jj} > 0.6, \quad (3.1)$$

where p_{Tj} is the transverse momentum of a final state jet and R_{jj} describes the separation of the two partons in the pseudo-rapidity η versus azimuthal angle plane.

In our simulation, we used the CTEQ4L set for parton-distribution functions [12], with a factorization scale equal to $\sqrt{p_{T1} p_{T2}}$ and we fixed $\alpha_s = 0.12$. We postpone any discussion on factorization- and renormalization-scale dependence to a further paper [6].

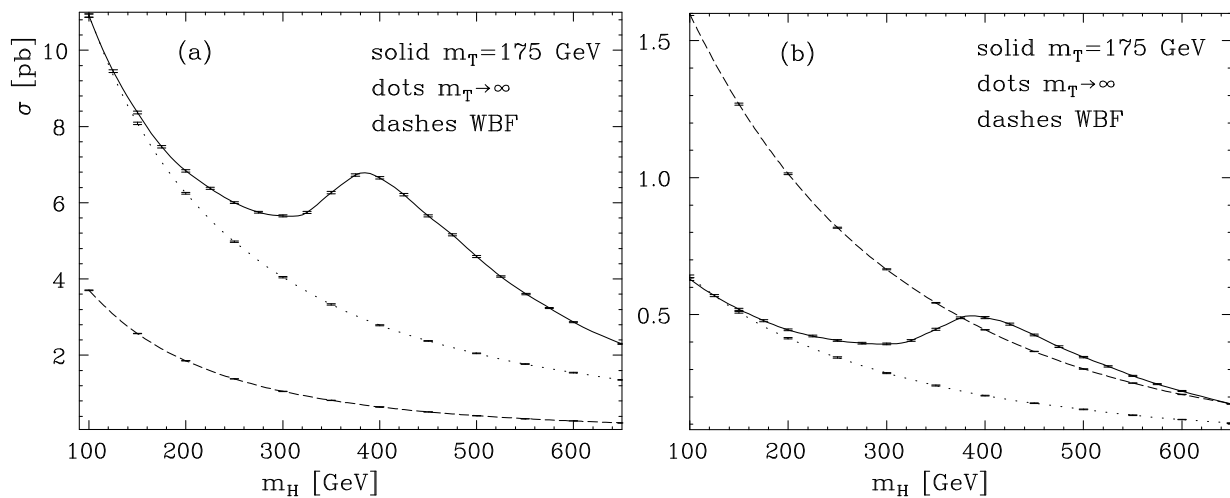


Figure 2: $H + 2$ jet cross sections in pp collisions at $\sqrt{s} = 14$ TeV as a function of the Higgs boson mass. Results are shown for gluon-fusion processes induced by a top-quark loop with $m_t = 175$ GeV and in the $m_t \rightarrow \infty$ limit, computed using the heavy-top effective Lagrangian, and for weak-boson fusion. The two panels correspond to two sets of jet cuts: (a) inclusive selection (see Eq. (3.1)) and (b) WBF selection (Eqs. (3.1) and (3.2)).

Expected $H + 2$ jet cross sections at the LHC are shown in Fig. 2, as a function of the Higgs boson mass, m_H . The three curves compare results for the expected SM gluon-fusion cross section at $m_t = 175$ GeV (solid line) with the large m_t limit (dotted line), and with the WBF cross section (dashed line). Error bars indicate the statistical errors of the Monte

Carlo integration. Cross sections correspond to the sum over all Higgs decay modes: finite Higgs width effects are included.

Figure 2 (a) shows cross sections within the minimal cuts of Eq. (3.1). The gluon-fusion contribution dominates because the cuts retain events with jets in the central region, with relatively small dijet invariant mass.

In order to assess background levels for WBF events it is more appropriate to consider typical tagging jet selections employed for WBF studies [13]. This is done in Fig. 2 (b) where, in addition to the cuts of Eq. (3.1), we require

$$|\eta_{j1} - \eta_{j2}| > 4.2, \quad \eta_{j1} \cdot \eta_{j2} < 0, \quad m_{jj} > 600 \text{ GeV}, \quad (3.2)$$

i.e. the two tagging jets must be well separated, with three units of pseudo-rapidity between the jet definition cones, they must reside in opposite detector hemispheres and they must possess a large dijet invariant mass. With these selection cuts the weak-boson fusion processes dominate over gluon fusion by about 3/1 for Higgs boson masses in the 100 to 200 GeV range. This means that a relatively clean separation of weak-boson fusion and gluon-fusion processes will be possible at the LHC, in particular when extra central-jet-veto techniques are employed to further suppress semi-soft gluon radiation in QCD backgrounds. A suppression by a factor three of gluon fusion as compared to WBF cross sections is to be expected with a central-jet veto [13].

A conspicuous feature of the $H + 2$ jet gluon-fusion cross sections in Fig. 2 is the threshold enhancement at $m_H \approx 2m_t$, an effect which is familiar from the inclusive gluon-fusion cross section. Near this “threshold peak” the gluon-fusion cross section rises to equal the WBF cross section, even with the selection cuts of Eq. (3.2). Well below this region, the large m_t limit provides an excellent approximation to the total $H + 2$ jet rate from gluon fusion, at least when considering the total Higgs production rate only. Near top-pair threshold the large m_t limit underestimates the rate by about a factor of 2.

A somewhat surprising feature of Fig. 2 (b) is the excellent approximation provided by the large m_t limit at Higgs boson masses below about 200 GeV. Naively one might expect the large dijet invariant mass, $m_{jj} > 600$ GeV, and the concomitant large parton center-of-mass energy to spoil the $m_t \rightarrow \infty$ approximation. This is not the case, however. The validity range of the $m_t \rightarrow \infty$ approximation is best appreciated in Fig. 3, where we show the transverse-momentum distribution of the harder of the two jets for an intermediate mass Higgs boson. At transverse momenta below 200 GeV the large m_t limit works extremely well. It is the large p_{Tj} region where this approximation breaks down. Small jet transverse momenta but large dijet invariant masses are well modeled by the large m_t limit.

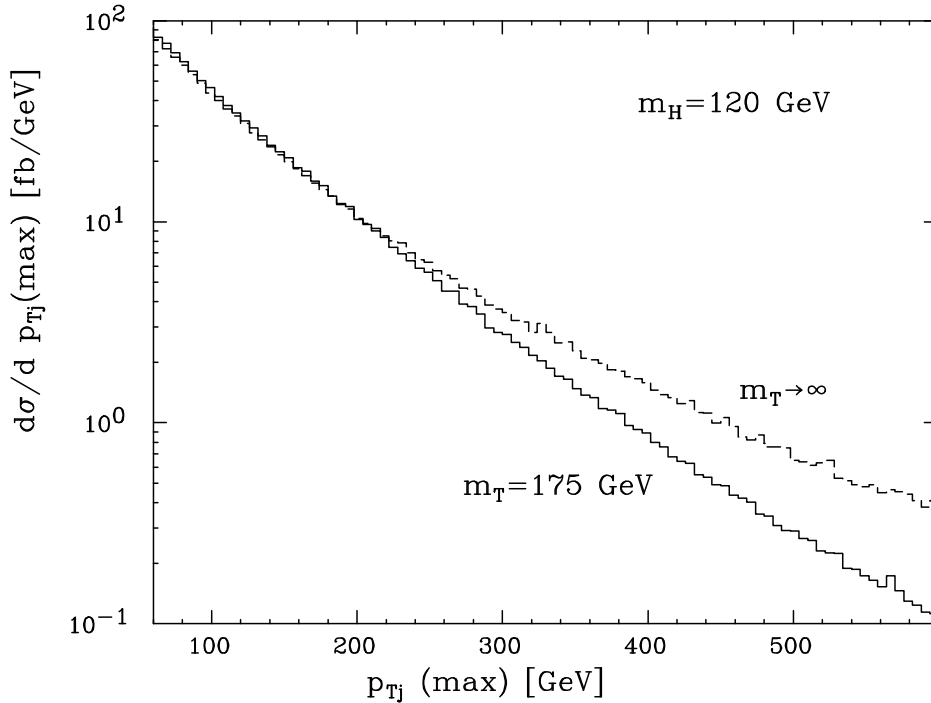


Figure 3: *Transverse-momentum distribution of the hardest jet in $H + 2$ jet events from gluon-fusion processes. Jets are defined via the inclusive selection of Eq. (3.1). The two curves are for $m_t = 175$ GeV and for the $m_t \rightarrow \infty$ limit, computed using the heavy-top effective Lagrangian. The mass of the Higgs is set to 120 GeV.*

4 Conclusion

In this letter we have provided first results of a full $\mathcal{O}(\alpha_s^4)$ calculation of $H + 2$ jet cross sections, including the analytic top-mass dependence. Event rates are sizable, of order 5 to 10 pb with minimal jet-selection cuts. With stringent forward-jet tagging cuts, as suggested for the Higgs search in weak-boson fusion, rates drop to about a third of the WBF rate, which implies that a relatively clean separation of gluon fusion and weak-boson fusion will be possible at the LHC. Sizable deviations from the large m_t limit are seen for Higgs boson masses of order $2m_t$ or for large jet transverse momenta. However, the large m_t limit works well for parton center of mass energies $\sqrt{\hat{s}} > 2m_t$, provided that $m_H \lesssim m_t$ and that the transverse momenta remain small compared to m_t .

Acknowledgements

C.S. acknowledges the U.S. National Science Foundation under grant PHY-0070443. W.K. acknowledges the DOE funding under Contract No. DE-AC02-98CH10886. This research was supported in part by the University of Wisconsin Research Committee with funds granted by

the Wisconsin Alumni Research Foundation and in part by the U. S. Department of Energy under Contract No. DE-FG02-95ER40896.

References

- [1] G. L. Bayatian *et al.*, CMS Technical Proposal, report CERN/LHCC/94-38 (1994); R. Kinnunen and D. Denegri, CMS NOTE 1997/057; R. Kinnunen and A. Nikitenko, CMS TN/97-106; R. Kinnunen and D. Denegri, hep-ph/9907291.
- [2] ATLAS Collaboration, ATLAS TDR, report CERN/LHCC/99-15 (1999).
- [3] D. Zeppenfeld, R. Kinnunen, A. Nikitenko and E. Richter-Was, Phys. Rev. D **62**, 013009 (2000) [hep-ph/0002036].
- [4] A. Djouadi, N. Spira and P. Zerwas, Phys. Lett. **B264**, 440 (1991); M. Spira, A. Djouadi, D. Graudenz and P.M. Zerwas, Nucl. Phys. **B453**, 17 (1995); S. Dawson, Nucl. Phys. **B359**, 283 (1991).
- [5] S. Catani, D. de Florian and M. Grazzini, hep-ph/0102227; R. Harlander and W. Kilgore, hep-ph/0102241.
- [6] V. Del Duca, W. Kilgore, C. Oleari, C. Schmidt and D. Zeppenfeld, in preparation.
- [7] G. Passarino and M. Veltman, Nucl. Phys. B **160**, 151 (1979).
- [8] G. 't Hooft and M. Veltman, Nucl. Phys. **B153**, 365 (1979).
- [9] A. Denner, U. Nierste and R. Scharf, Nucl. Phys. **B367**, 637 (1991).
- [10] Z. Bern, L. Dixon and D. Kosower, Phys. Lett. **B302**, 299 (1993), Erratum-ibid. **B318**, 649 (1993) [hep-ph/9212308]; Z. Bern, L. Dixon and D. Kosower, Nucl. Phys. **B412**, 751 (1994) [hep-ph/9306240].
- [11] S. Dawson, R.P. Kauffman, Phys. Rev. Lett. **68**, 2273 (1992); R.P. Kauffman, S.V. Desai, D. Risal, Phys. Rev. **D55**, 4005 (1997), Erratum-ibid. **D58**, 119901 (1998) [hep-ph/9610541].
- [12] H.L. Lai *et al.*, Phys. Rev. **D55**, 1280, (1997) [hep-ph/9606399].
- [13] D. Rainwater, R. Szalapski and D. Zeppenfeld, Phys. Rev. **D54** 6680 (1996); D. Rainwater and D. Zeppenfeld, Phys. Rev. **D60**, 113004 (1999), Erratum-ibid. **D61**, 099901 (2000); D. Rainwater, PhD thesis, hep-ph/9908378; T. Plehn, D. Rainwater and D. Zeppenfeld, Phys. Rev. **D61**, 093005 (2000).